LAWRENCE
LIVERMORE
NATIONAL
LABORATORY

LLNL-JRNL-482754

Computing and Partitioning Cloud Feedbacks using Cloud Property Histograms. Part I: Cloud Radiative Kernels

M. D. Zelinka, S. A. Klein, D. L. Hartmann

May 4, 2011

Journal of Climate

Disclaimer

This document was prepared as an account of work sponsored by an agency of the United States government. Neither the United States government nor Lawrence Livermore National Security, LLC, nor any of their employees makes any warranty, expressed or implied, or assumes any legal liability or responsibility for the accuracy, completeness, or usefulness of any information, apparatus, product, or process disclosed, or represents that its use would not infringe privately owned rights. Reference herein to any specific commercial product, process, or service by trade name, trademark, manufacturer, or otherwise does not necessarily constitute or imply its endorsement, recommendation, or favoring by the United States government or Lawrence Livermore National Security, LLC. The views and opinions of authors expressed herein do not necessarily state or reflect those of the United States government or Lawrence Livermore National Security, LLC, and shall not be used for advertising or product endorsement purposes.

Computing and Partitioning Cloud Feedbacks using Cloud Property Histograms.

Part I: Cloud Radiative Kernels

Mark D. Zelinka *

Department of Atmospheric Sciences, University of Washington, Seattle, Washington,

and Program for Climate Model Diagnosis and Intercomparison, Lawrence Livermore National Laboratory, Livermore, California

Stephen A. Klein

Program for Climate Model Diagnosis and Intercomparison, Lawrence Livermore National Laboratory, Livermore, California

Dennis L. Hartmann

Department of Atmospheric Sciences, University of Washington, Seattle, Washington

* *Corresponding author address:* Mark D. Zelinka, Program for Climate Model Diagnosis and Intercomparison Lawrence Livermore National Laboratory 7000 East Avenue, L-103 Livermore, CA 94551
E-mail: zelinka1@llnl.gov

ABSTRACT

In this study we propose a novel technique for computing cloud feedbacks using histograms of cloud fraction as joint functions of cloud top pressure (CTP) and optical depth (τ). These histograms were generated by the International Satellite Cloud Climatology Project (ISCCP) simulator, which was incorporated into doubled CO_2 equilibrium slab ocean model experiments as part of the first phase of the Cloud Feedback Model Intercomparison Project (CFMIP1). We use a radiative transfer model to compute top of atmosphere (TOA) flux sensitivities to cloud fraction perturbations in each bin of the ISCCP simulator histogram, which we refer to as a cloud radiative kernel. Multiplying the cloud radiative kernel histogram with the histogram of actual cloud top fraction changes per unit of global warming simulated by each model produces an estimate of cloud feedback. Unlike previous studies in which the types of cloud changes that contribute to cloud feedback are indirectly inferred, this technique allows more direct attribution of the feedback to the cloud types from which it arises.

In five of the six models for which the comparison is possible, both the spatial structures and globally integrated values of cloud feedbacks computed in this manner agree remarkably well with those computed by adjusting the change in cloud radiative forcing for non-cloud related effects as in Soden et al. (2008). We show that the global mean model-simulated cloud feedback in the full ensemble of ten models is dominated by contributions from changes in medium thickness ($3.6 \leq \tau < 23$) cloud fractions, but that changes in the fractional coverage of thick ($\tau \geq 23$) clouds bring about the rapid transition from positive to negative cloud feedback poleward of about 50°. High ($CTP < 440$ hPa) cloud changes are the dominant contributor to LW cloud feedback at every latitude, but because their impacts on LW and SW cloud feedback are in opposition, they contribute less to the net cloud feedback than do the

positive contributions from low ($CTP \geq 680$ hPa) cloud fraction reductions. Surprisingly, middle ($440 \leq CTP < 680$ hPa) level cloud reductions are responsible for positive SW cloud feedbacks that are nearly 70% of the size of those due to low clouds. Furthermore, more than half of the global mean net cloud feedback can be attributed to the combined response of middle- and high-level clouds. Finally, high cloud changes induce wider range of LW and SW cloud feedbacks across models than do low clouds, providing a caution against solely attributing large uncertainty in cloud feedback to low clouds.

1. Introduction

Clouds are fundamentally important to the energy budget of the planet owing to their high albedo, large emissivity, and location at colder temperatures than the surface. Relative to a hypothetical cloudless but otherwise identical planet, the global and annual mean effect of clouds at the top of atmosphere (TOA) is to increase the amount of reflected shortwave (SW) radiation by 48 W m^{-2} and to reduce the amount of emitted longwave (LW) radiation by 31 W m^{-2} (Harrison et al. (1990)). Thus the net effect of clouds, which is the sum of these large and opposing effects, is to cool the planet by 17 W m^{-2}.

An important question of climate science whose answer remains largely unconstrained is how cloud radiative effects will change as the planet warms due to long-lived greenhouse gases. A change in clouds that is systematically associated with an increase in global mean surface temperature represents a feedback in which the radiation imbalance at the TOA due to increased greenhouse gas concentrations is amplified or dampened. The current generation of global climate models (GCMs) all exhibit positive cloud feedbacks (Soden and

Held (2006)), indicating that modeled clouds change in such a way as to cool the planet less as the planet warms. However, the inter-model spread in cloud feedback is larger than for any other feedback process and is the primary contributor to the large range of climate sensitivity produced by the models (e.g., Cess (1990); Soden and Held (2006); Ringer et al. (2006)).

Uncertainty in cloud feedback must be reduced if the range of possible future climates simulated by models is to be narrowed. To do so, it is necessary to identify the nature of cloud changes that give rise to cloud feedbacks within models, with an eye towards identifying those aspects that are robust from those that are not robust. Such an approach may begin to separate the physical processes that are well understood, better constrained, and/or consistently modelled from those that are not. This requires accurate methods to quantify cloud feedback that can be applied across models using the available diagnostics archived by the modeling centers.

Three primary methods have been used previously to attribute cloud feedbacks to the cloud changes from which they arise. Bony et al. (2004), Bony and Dufresne (2005), and Wyant et al. (2006) used 500 hPa vertical motion as a proxy for the large-scale circulation to separate the response of tropical clouds to an imposed climate change into a thermodynamic component due to intrinsic temperature dependence of cloud radiative properties and a dynamic component due to changes in circulation. Webb et al. (2006) inferred the types of cloud changes that are consistent with the relative strengths of the changes in LW and SW cloud forcing at each gridpoint. Williams and Tselioudis (2007) and Williams and Webb (2009) employed a clustering technique to define several primary cloud regimes from ISCCP simulator output and assessed the contributions to cloud feedback from changes in

the relative frequency of occurrence of each regime and from changes in the cloud radiative forcing within each regime. All of these studies found a dominant role for low clouds (defined by Bony et al. (2004) as those in regimes of moderate subsidence, by Webb et al. (2006) as those for which the change in LW cloud forcing is small but the change in SW cloud forcing is large, and by Williams and Tselioudis (2007) and Williams and Webb (2009) as stratocumulus and stratocumulus-to-cumulus transition regimes) in driving the inter-model spread in net cloud feedback. However, two important ambiguities remain in all of these studies.

First, Soden et al. (2004) have demonstrated that the change in cloud forcing, defined as the difference between clear- and all-sky TOA fluxes (e.g., Charlock and Ramanathan (1985)), may not be an accurate measure of the magnitude or even the sign of the cloud feedback because it includes non-cloud-induced changes in fluxes that are irrelevant for cloud feedback. This is especially true at high latitudes where large reductions in surface albedo may incorrectly imply large negative SW cloud feedback, but is also important in deep convective regions where the emission from clouds remains nearly fixed, falsely implying a near-zero LW cloud feedback when in reality it is moderately positive (Zelinka and Hartmann (2010)). (Soden et al. (2008) proposed a method to compute cloud feedbacks that accounts for and attempts to remove the effect of clear-sky changes on the change in cloud forcing, which is discussed below.)

The second important ambiguity in these studies is that – even if clear-sky effects are accounted for – the use of such an integrated quantity as the change in radiation at the TOA does not allow for clear identification of the nature of cloud changes from which the radiative changes arise. For example, at a location in which the change in both SW and LW cloud

forcing is positive (i.e., one given the H classification of Webb et al. (2006)), the implied cloud response is "less/thinner low and more/higher/thicker high thin cloud." Clearly a number of plausible cloud responses can give rise to a particular combination of LW and SW cloud forcing changes. Another arguably vague finding that is common to these studies is the small role of high clouds in contributing to both the mean and inter-model spread in cloud feedback. Is this because high clouds exhibit little change, and do so similarly across models, or because there are large but compensating changes in high clouds (e.g., large upward shifts and large reductions in coverage) that occur consistently across models? Such integrated measures potentially mask competing effects of cloud changes, which may give a false indication of robustness or de-emphasize the importance of a particular type of cloud change. Therefore it is preferable to devise an alternative method in which the cloud changes that cause the cloud feedback can be determined directly.

In this paper we propose a different technique for attributing the contributions of specific types of cloud changes to cloud feedback that makes use of histograms of cloud fraction partitioned by cloud top pressure (CTP) and visible optical depth (τ), along with corresponding histograms containing TOA radiative flux sensitivities to cloud fraction changes. The CTP-τ histograms of cloud fraction we use are generated by the ISCCP simulator (Klein and Jakob (1999); Webb et al. (2001)), which was run inline in GCMs as part of the experiments performed for the first phase of CFMIP (McAvaney and Le Treut (2003)). The simulator provides a plausible distribution of cloud top fractions more directly related to the cloud top information that passive satellite sensors observing the model atmosphere would retrieve. Because the cloud top fractions are individually "visible" from space and are therefore individually impacting the TOA radiative fluxes, it is possible to compute a

cloud radiative kernel that describes the TOA flux sensitivity to cloud top fraction changes in the histogram. We note that the simulator is essential as our technique cannot be applied to conventional GCM output because of the invalidity of the assumption that TOA flux sensitivities to cloud amount perturbations in individual layers can be added linearly to compute the net TOA flux anomaly [1]. By providing a decomposition of the full cloud field into its individual radiatively-relevant components, the ISCCP simulator removes the uncertainties associated with overlap assumptions and cloud radiative properties that preclude the construction of a cloud radiative kernel from conventional GCM output.

Our method allows us to assess the cloud types (e.g., high vs. low, thin vs. thick) most responsible for the mean and spread of the feedback at any given location, just as the radiative kernels of Soden et al. (2008) made it is possible to identify the tropical upper troposphere as a region of primary importance to the water vapor feedback. This provides an avenue to identify the cloud types of greatest importance and quantify their effect on cloud feedbacks in different regions, and perhaps guide future efforts to find the causes of cloud changes. As in the case of the radiative kernels for temperature, water vapor, and surface albedo of Soden et al. (2008), the cloud radiative kernels computed here are appealing for two reasons in part. First, they are easy to use because they are applied to monthly mean model ISCCP

[1] The radiative impact at the TOA of, for example, a 1% increase in cloud amount at some height depends critically on the amount and type of cloud above and below this level, and will vary on a case-by-case basis. This is primarily because clouds are nearly black in the IR, which means that even small perturbations at a given level impact the radiation elsewhere. The impact of clouds is further complicated by the variety of cloud overlap assumptions in models which determine what portion of clouds at a given level is "visible" from space. Furthermore, cloud amount is not the only relevant property affecting TOA fluxes: Cloud radiative properties such as LW emissivity and visible optical depth significantly impact fluxes, making a radiative kernel derived simply from cloud amount perturbations useless. Thus nonlinearities in the impact of clouds on radiative fluxes preclude the construction of a cloud radiative kernel from layer-by-layer perturbations of clouds in a manner similar to that employed by Soden et al. (2008) to compute temperature, water vapor, and surface albedo kernels. While strictly this is true for temperature and water vapor perturbations as well, the nonlinearities in radiative transfer are much smaller than those associated with clouds.

simulator output. This avoids having to compute cloud changes from instantaneous output as must be done for the cumbersome partial radiative perturbation method of Wetherald and Manabe (1988). Second, they are appealing because the part of the feedback calculation that depends on the radiation code is calculated by a single radiation code, thereby providing a standard that can be applied across models. Thus the cloud radiative kernels can be used to directly attribute cloud feedbacks to the responses of individual cloud types. Ultimately, this will provide for a more detailed assessment of robust and non-robust cloud responses across models, which could provide an avenue for assessing the realism of cloud responses and therefore narrowing the range of uncertainty in cloud feedback estimates.

In the first part of this paper we document the method of computing the TOA radiative impact of cloud fraction perturbations in each bin of the CTP- and τ-partitioned histogram using a radiative transfer code. We will refer to this as a cloud radiative kernel. Then, multiplying the cloud radiative kernel histogram with the change in cloud fraction histogram per unit of global mean surface temperature change between a control and doubled CO_2 climate, we compute the cloud feedbacks in the CFMIP simulations. To build confidence in our method, we demonstrate that the feedback computed from ISCCP simulator output compares remarkably well with the adjusted change in cloud forcing method of Soden et al. (2008), both in the global mean sense and on a point-by-point basis. The advantage of this technique, however, is that it allows for unambiguous quantitative attribution of the cloud types that contribute to the feedback at every location across models. We do not *infer* the cloud responses that are consistent with the change in cloud forcing at each location but rather *compute* the cloud feedback directly from the change in cloud distribution. Finally, we finish with a brief survey of results related to the partitioning of cloud feedbacks at

different altitude levels and different optical depths followed by the main conclusions of this first paper.

In Part II of this work (Zelinka et al. 2011b, manuscript submitted to *J. Climate*), we propose a simple method of decomposing the cloud changes that allows us to distinguish between and separately quantify the contribution to cloud feedback from changes in the cloud fractional area coverage and the distribution of cloud altitude and optical depth.

2. Data

We make use of output from slab ocean simulations performed in twelve models as part of the CFMIP experiments (McAvaney and Le Treut (2003)) and submitted to the IPCC AR4 archive (Table 1). Experiments are separately run to equilibrium for a control climate with preindustrial CO_2 and a perturbed climate with doubled CO_2. We compute a monthly mean annual cycle from the last 20 years of each run, and difference them to compute feedbacks. All model output is regridded onto the grid corresponding to that of the radiative kernels of Soden et al. (2008). The *bmrc1*, *gfdl_mlm2_1*, *ipsl_cm4*, *miroc_hisens*, *mpi_echam5*, and *ncar_ccsm3_0* models did not archive specific humidity and/or temperature, making it impossible to compute cloud feedbacks from the adjusted change in cloud radiative forcing of Soden et al. (2008). For the models in which it is possible to calculate the adjusted change in cloud radiative forcing, we use the values given in Figure 1a of Webb et al. (2006) for the radiative forcing due to doubling CO_2: 3.75 W m^{-2} K^{-1} for the *ukmo_hadsm4*, *ukmo_hadsm3*, and *ukmo_hadgsm1* models, 3.6 W m^{-2} K^{-1} for the *uiuc* model, 3.1 W m^{-2} K^{-1} for the *miroc_losens* model, and the mean of these three values for the *cccma_agcm4_0*

model. The cloud masking of the CO_2 forcing is assumed to be 16%, as in Soden et al. (2008), and no forcing is assumed to be present in the SW.

In all of the CFMIP models, ISCCP simulators are run inline during integration to produce distributions of cloud top fraction as functions of CTP and τ. We will refer to the cloud fraction as a function of CTP and τ within the histogram as C and its change as ΔC. Early versions of the ISCCP simulator are described in detail in Klein and Jakob (1999) and Webb et al. (2001). Briefly, the ISCCP simulator produces an estimate of the cloud distribution as a function of CTP and τ that is consistent with how a satellite-borne passive sensor would retrieve an atmospheric column with the properties produced by the model. Account is taken of the limitations and biases that exist in ISCCP retrievals of cloud properties such as the ability to only observe these distributions in sunlit conditions, the ability to only observe the highest cloud top in the case of multi-layered clouds, and the tendency for ISCCP retrievals to overestimate CTP for very thin clouds overlying thicker clouds. Using the overlap assumption in each model allows for an estimate of the total cloud fraction in each CTP and τ bin in a manner similar to the ISCCP retrieval algorithm that assigns cloud fractions as the fraction of pixels in a 280 km region that correspond to a particular CTP and τ category. Unlike the cloud fraction diagnostics provided by each individual modeling center that are defined according to each model's cloud scheme, cloud fractions produced by the ISCCP simulator are defined consistently across models. This consistency is essential for using cloud diagnostics to compute cloud feedbacks across an ensemble of models using the technique outlined below. (Note that inconsistencies were found in the implementation of the simulator by some modelling groups; our methods of correction and rationale for choosing one model to exclude are described in the Appendix.)

While this will be a significant advance in our ability to diagnose cloud feedbacks from models, one must acknowledge the limitations of using ISCCP simulator output to diagnose cloud feedbacks. Known limitations include the finite resolution of the ISCCP histograms, the lack of diagnosis of cloud property changes from the dark half of the planet which might affect the LW cloud feedback, and the fact that the reported cloud changes may be due to clouds at significantly lower levels than the reported cloud-top pressure of the highest cloud in the column. These limitations can be expected to play some role in our ability to partition cloud feedback to cloud types; however, they are not likely to substantially negate the value of these calculations nor the fact that the ISCCP simulator remains the best possible to way to analyze cloud property feedbacks in the CFMIP1 archive.

3. Computation of Cloud Radiative Kernels

To assess the role of changes in histogram-partitioned cloud fraction (ΔC) on the TOA radiative fluxes, we first compute histograms of overcast sky cloud radiative forcing in a manner similar to that described in Hartmann et al. (2001) and Kubar et al. (2007). Unlike those studies, we use zonal and monthly mean model fields of temperature and water vapor that are computed from the annual cycles of the control runs of models 1-6 as input to the Fu-Liou radiation code (Fu and Liou (1992)). We assume a spatially-invariant surface emissivity of 0.99, uniform CO_2, CH_4, and N_2O mixing ratios of 330, 1.6, and 0.28 ppmv, respectively, a standard profile of ozone mixing ratio, and a solar constant of 1366 W m^{-2}.

The first step in constructing the overcast-sky cloud forcing histogram at any given location and time is to calculate clear-sky TOA LW and SW fluxes. "Clear sky" simply

means we set liquid water content and ice water content to zero throughout the column in the radiative transfer model. Then, the Fu-Liou code is run again 49 times, once for each of the seven CTP and seven τ bins, each time placing a cloud in the column with properties corresponding to the midpoints of each τ-CTP bin. The TOA fluxes computed by the code for each bin of the histogram are then subtracted from the clear-sky flux to compute a histogram of overcast-sky cloud forcing which represents the impact of each cloud type on the TOA radiative fluxes relative to clear skies.

Clouds are "inserted" into the atmospheric column of the radiative transfer model by setting liquid or ice water content to nonzero values between the cloud top and base, with the geometric thickness determined using empirical relationships between cloud top temperature and τ given in Minnis et al. (2011, manuscript submitted to *IEEE Trans. Geosci. Remote Sens.*). Clouds with tops warmer than 263 K are assumed to be liquid, with a constant liquid water content throughout the cloud equal to the liquid water path divided by the cloud geometric thickness. We compute the liquid water path using τ and Equation 1 of Slingo (1989) with the assumption of a constant effective radius of 10 μm. For clouds with tops colder than 263 K, we compute ice water content using the parameterization of extinction coefficient in terms of ice water content and generalized effective ice crystal size given in Equation 3.9a of Fu (1996). The extinction coefficient, which we assume is constant throughout the depth of the cloud, is simply the optical depth divided by the cloud geometric thickness. We compute the generalized effective size using Equation 3.12 of Fu (1996) with an assumed effective radius of 30 μm. Because we assume both the extinction coefficient and effective radius are constant, the ice water content is also constant throughout the depth of the cloud.

Our fairly crude parameterization of clouds would likely be inappropriate for correctly computing the impact of clouds on atmospheric radiative heating rates or radiative fluxes at the surface. However, our goal is only to compute TOA fluxes that are realistic for clouds with given gross features. It is less important whether the vertical structure of cloud properties is highly realistic, as long as the cloud top temperature and the total optical depth are correctly represented in the radiation code.

To accurately capture the diurnal range of incident solar radiation, TOA fluxes with and without clouds are computed for the zenith angles for each of 24 hours of a day and then averaged before being differenced. We use the 24 zenith angles appropriate for each month and latitude, using a day in the middle of each month. Though our use of zonal mean profiles of temperature and humidity does not allow us to take into account any longitude dependence that may impact the clear-sky fluxes, we do account for spatial differences in surface albedo by performing every calculation 10 times, one for each of ten surface albedo bins between 0 and 1. This will allow us to account for the spatial variation in SW cloud forcing that comes simply from variations in surface albedo that impact clear-sky fluxes (i.e., unrelated to clouds). In sum, we generate a LW and SW overcast sky cloud forcing histogram for every latitude and month, and for ten evenly-spaced surface albedo bins between 0 and 1.

Because the computation of cloud forcing in each bin of the histogram is performed using a single atmospheric column with only that cloud type present, we refer to it as an overcast-sky cloud forcing histogram. Dividing the radiative forcings by 100 expresses the values in units of W m^{-2} %$^{-1}$. The computed histogram is a cloud radiative kernel (K) giving the

sensitivity of TOA fluxes (R) to perturbations in cloud fraction as functions of CTP and τ:

$$K \equiv \frac{\partial R}{\partial C}. \tag{1}$$

As in the case of the standard temperature and water vapor radiative kernels of Soden et al. (2008), the cloud radiative kernel depends on latitude and month. It is slightly different in that we did not compute a kernel for each longitude but we did compute a separate kernel for each of ten surface albedo bins. Our computation is much simpler than that of Soden et al. (2008), as we input zonal mean monthly mean thermodynamic profiles averaged across six models into the Fu Liou code, whereas they called the GFDL model's radiation code 8 times daily at every location on the planet for each perturbation level and quantity for a 1-year simulation to compute a TOA flux sensitivity to tiny perturbations. Certainly more accurate methods of computing the cloud radiative kernels could be performed than is performed here, but we demonstrate in this paper that our technique is useful and quite accurate.

In Figure 1, we show the global and annual mean of the cloud radiative kernels. The LW cloud radiative kernel is positive for all cloud types, indicating that an increase in cloud fraction results in a decrease in outgoing longwave radiation (OLR), and vice versa. The magnitude of the kernel is sensitive to both τ and CTP. For thin clouds (τ<3.6), OLR is sensitive to changes in both their optical depth and their vertical distribution, but for clouds with τ>3.6, the sensitivity of OLR to changes in the optical depth distribution becomes saturated and OLR is solely impacted by changes in the vertical distribution. Conversely, the SW cloud radiative kernel is negative for all cloud types, indicating that increases (decreases)

in cloud fraction result in increased (decreased) SW reflection to space. The impact of cloud fraction changes is much greater for thick clouds but does not depend strongly on CTP. The small dependence on CTP exhibited in the SW cloud radiative kernels is most likely due to the decreasing attenuation of SW radiation by above-cloud gaseous absorption with decreasing CTP.

Generally, a shift in the cloud distribution towards higher and thinner bins results in a positive (warming) impact on net TOA fluxes. However, note that the largest positive net flux sensitivity is for increases in cloud fraction for τ between 1.3 and 3.6 (see also Fig. 13b of Ackerman et al. (1988)). A shift in the distribution towards lower and thicker clouds negatively impacts the net TOA fluxes because of increased SW reflection and LW emission.

4. Computation of Cloud Feedback Using Cloud Radiative Kernels

Multiplying the cloud radiative kernel histogram (K) by the histogram of the change in cloud fraction (ΔC) gives an estimate of the contribution of each cloud type to the change in TOA radiation associated with climate change (in this case, a doubling of CO_2):

$$\Delta R = K * \Delta C. \tag{2}$$

For a given location and month, ΔC is multiplied by the cloud radiative kernel histogram that corresponds to the control climate's clear-sky surface albedo for that location and

month. Because the kernel is computed using the atmospheric and surface conditions from the control climate, the change in TOA fluxes computed in this manner is due solely to the change in clouds (i.e., no clear sky flux changes are included), which is the quantity relevant for cloud feedback. Dividing this response by the change in global mean temperature ($\Delta\overline{T_s}$) provides an estimate of the cloud feedback due to each cloud type (f):

$$f = \frac{\Delta R}{\Delta\overline{T_s}}. \tag{3}$$

Note that both f and ΔR are matrices. Summing the resultant histogram over all cloud types produces an estimate of the local contribution to the cloud feedback, which can then be integrated over the entire planet to compute the global mean cloud feedback.

Before discussing our cloud feedback results, we wish to note that hereafter we refer to the radiative perturbations brought about by cloud changes as cloud feedback, with the implicit assumption that the simulated changes in clouds evolve with the change in global mean surface temperature. Gregory and Webb (2008) have provided evidence that a portion of the cloud-induced radiation response that is typically considered cloud feedback actually occurs due to very rapid tropospheric adjustment following a step change in CO_2 concentration, and that the component of cloud change that evolves with temperature is less than expected in most models. Colman and McAvaney (2011) have confirmed this effect in the CAWCR (formerly BMRC) model, but note that it primarily affects the SW cloud amount feedback, whereas other cloud feedbacks generally behave in the classical sense. Our analysis does not distinguish between cloud changes that emerge with increasing global mean temperature and those that occur rapidly due to doubling of CO_2; thus what we refer to as cloud feedback

may in some cases be a combination of these effects. Separating these components is not possible with the experiments performed in CFMIP1; it will be possible with experiments currently being performed for CFMIP2.

In the left column of Figure 2 we show histograms of (a) 1xCO_2 and (b) 2xCO_2 global mean cloud fraction of the *ukmo_hadsm4*, *ukmo_hadsm3*, *ukmo_hadgsm1*, *miroc_losens*, and *cccma_agcm4_0* models, along with (c) their difference expressed per unit change in each model's global mean surface temperature between the two states. The *uiuc* model is excluded for reasons discussed below. Global mean cloud fraction decreases in these models by 0.38% K^{-1} on average, with the reductions in cloud fraction occuring in a majority of CTP and τ bins. Large reductions in cloud fraction occur in the highest CTP bin (i.e., the lowest clouds) in the 0.3 - 9.4 optical depth range. Cloud fraction increases in the lowest CTP bin (i.e., the highest clouds) at all optical depths except for τ between 0 and 0.3. Cloud fraction also increases in the 680-1000 hPa CTP bins for optical depths greater than 23 and in the 180-310 hPa CTP bin for optical depths greater than 3.6.

Multiplying the ΔC histogram with the LW, SW, and net K histograms shown in Figure 1 produces a histogram showing the contribution of each cloud type to the respective feedbacks (Figure 2d, e, and f). Note that the multiplication occurs for each location and month and is then averaged for this figure. The large increases in cloud fraction in the upper troposphere project strongly onto the LW cloud radiative kernel, which is most sensitive to cloud fraction changes in the lowest CTP bins. Where cloud fractions increase, the contribution to the LW cloud feedback is positive, and vice versa. Cloud fraction increases, primarily those occurring in the lowest CTP bin (i.e., the highest clouds), contribute 0.54 W m^{-2} K^{-1} to the LW cloud feedback, while cloud fraction decreases reduce the LW cloud feedback by 0.27

W m^{-2} K^{-1}, resulting in a LW cloud feedback due to all cloud fraction changes of 0.27 W m^{-2} K^{-1}.

Zelinka and Hartmann (2010) showed that the tendency for tropical (30°S-30°N) clouds to rise contributed significantly to the LW cloud feedback, but that high cloud fraction also systematically decreased as the planet warmed. They found that while high cloud fractional changes were important for changes in LW fluxes locally, the net effect over the entire Tropics was rather small and positive. The effect of high cloud reduction on the tropical mean LW cloud feedback may have been small because the decreases preferentially impacted thin clouds that have a smaller influence than thicker clouds on LW cloud forcing. Here we can quantify these competing effects. Hereafter we will use the ISCCP cloud classifications of Rossow and Schiffer (1999), namely low: $680 \leq CTP < 1000$ hPa, middle: $440 \leq CTP < 680$ hPa, high: $50 \leq CTP < 440$ hPa, thin: $\tau < 3.6$, medium: $3.6 \leq \tau < 23$, and thick: $\tau \geq 23$. Averaged across all models excluding *uiuc* and *mpi_echam5* (for reasons discussed below and in the Appendix), the change in tropical high cloud fraction is -0.03% K^{-1}, with thin, medium, and thick cloud changes equal to -0.04, 0.01, and slightly less than 0% K^{-1}, respectively. Tropical high cloud changes alone contribute 0.26 W m^{-2} K^{-1} to the LW cloud feedback, with thin, medium, and thick cloud changes contributing 0.05, 0.12, and 0.09 W m^{-2} K^{-1}, respectively. Note that even though thin and thick high cloud fractions decreased, their contributions to the LW cloud feedback are positive because of increased cloud altitude that manifests itself as increased cloud fraction in the 50-180 hPa bin and decreased cloud fraction in the 180-310 hPa bin. These results show that decreases in tropical high clouds are substantial, but because the reductions are primarily in thinner, warmer clouds, their combined net effect is a positive contribution to the LW cloud feedback, as found in Zelinka

and Hartmann (2010) for the fully coupled GCMs. A more complete decomposition of the LW cloud feedback into the components due to changes in cloud altitude, optical depth, and fraction will be presented in Part II.

In contrast to the LW cloud feedback, cloud changes throughout the depth of the troposphere contribute to the SW cloud feedback, with large positive contributions coming from bins in which cloud fractions decrease, and vice versa. Cloud fraction changes project more strongly onto the SW cloud radiative kernel if they occur at higher optical depths; thus the effect of cloud fraction changes in the lowest τ bins are largely irrelevant for the SW cloud feedback.

The net cloud feedback histogram shares features of both the LW and SW histograms, but is largely dominated by the positive SW cloud feedback for all pressures greater than about 310 hPa due to reductions in low and mid-level cloud fraction. At pressures less than 310 hPa, LW and SW cloud feedback components compete against each other for dominance. The increase in cloud fraction in the lowest CTP bin contributes more strongly to the positive LW cloud feedback than to the negative SW cloud feedback for intermediate optical depths, but the opposite is true for thick high clouds. In the end, large reductions in middle- and low-level clouds that strongly reduce the amount of reflected radiation, coupled with increases in high level clouds that strongly reduce the amount of emitted LW radiation results in a net cloud feedback of 0.71 W m^{-2} K^{-1}. Considering that the average combined water vapor plus lapse rate feedback is 0.63 W m^{-2} K^{-1} in this ensemble, the net cloud feedback is quite strong.

5. Effectiveness of the Cloud Radiative Kernel Method in Computing Cloud Feedback

In this section we compare the cloud feedback computed using the cloud radiative kernels applied to ISCCP simulator output with the cloud feedback computed according to Soden et al. (2008). The latter technique involves adjusting the change in cloud radiative forcing by the amount of cloud masking that occurs in the other feedbacks and in the radiative forcing. Only the *ukmo_hadsm4*, *ukmo_hadsm3*, *ukmo_hadgsm1*, *uiuc*, *miroc_losens*, and *cccma_agcm4_0* models archived enough data to compute the adjusted change in cloud radiative forcing; thus we can only compare the two methods for those models.

In Figure 3 we show a point-by-point comparison of the LW and SW cloud feedbacks computed using cloud radiative kernels with those computed by the adjusted change in cloud radiative forcing method. Each point represents the feedback computed for a single month at a single location in the model, and locations in which the magnitude of the change in clear-sky surface albedo exceeds the 90th percentile have been removed (for reasons discussed below). Values of both LW and SW cloud feedback computed using the cloud radiative kernels developed here compare remarkably well on a point-by-point basis with values computed by adjusting the change in cloud radiative forcing. The regression slopes for every model are generally close to unity, with the exception of the SW cloud feedback comparison in the *uiuc* model. Large R^2 values for all but the *miroc_losens* model indicate that these two measures are highly correlated. Relative to the adjusted change in SW cloud radiative forcing ($SWCF$), the cloud radiative kernel calculation tends to overestimate the magnitude of both positive and negative SW cloud feedbacks, as the slopes in panels g-l are all ≥ 1. Although

still large for every model except *miroc_losens*, the R^2 values are systematically lower for the comparisons of LW cloud feedback than for the comparisons of SW cloud feedback in every model. The somewhat larger slope in panel f likely reflects our choice to rescale the LW kernel in the same manner as the SW kernel for the *cccma_agcm4_0* model, when a different scaling may be more appropriate (see the Appendix). Similarly, the slope between estimates of LW and SW cloud feedbacks cloud kernel-derived estimates and adjusted change in cloud forcing-derived in the *uiuc* model deviate substantially from unity, but the cause of this discrepancy remains unclear. Finally, the somewhat lower correlation between the two measures of cloud feedback for the *miroc_losens* model may arise in part because of mis-matches between the archived diagnostics in this model. Temperature and humidity profiles are archived only over the first 15 years of the $2xCO_2$ run, while the histogram is only archived over the last 5 years of the run (i.e., they are archived for non-overlapping time periods). Thus, the adjusted change in cloud forcing is computed using differences between two climate states that are different from the two climate states used to compute cloud feedback with the cloud kernels in the *miroc_losens* model.

Our comparisons between the two methods indicated poor agreement in some models over regions in which clear-sky surface albedo changes significantly between the two climate states. Visual inspection of feedback maps (not shown) indicated that a large percentage of these points came from high latitude regions where the adjusted change in cloud forcing method produced anomalous SW cloud feedbacks surrounded by regions with oppositely-signed SW cloud feedbacks. The cloud radiative kernel technique, on the other hand, exhibited a relatively "smooth" geographic distribution of feedback values at high latitudes that is arguably more realistic. There are reasons to expect the adjusted change in cloud

forcing method to produce spurious cloud feedback values over regions in which clear-sky surface albedo changes substantially. Consider a hypothetical sunlit region with sea ice in the control climate but with no sea ice in a warmed climate and assume *no* change in clouds whatsoever. Since the cloud feedback is calculated as the impact of cloud changes on TOA radiation with everything else fixed, by definition, cloud feedback should be zero. The change in $SWCF$, conversely, will be negative because of the increased contrast between clear and all sky SW fluxes. The cloud kernel method proposed here will easily calculate zero cloud feedback because the kernel is being multiplied by a change in cloud fraction histogram containing zeros. In order for the adjusted change in $SWCF$ to equal zero requires an almost miraculous positive adjustment made up of contributions from how much the surface albedo and SW water vapor feedbacks are masked by clouds. This miraculous adjustment is nearly impossible since the all-sky radiative kernels used to compute cloud masking are informed only by the clouds that are present in the GFDL model. Any difference between the mean state cloud fields in the model in which the kernel is applied and those of the model in which the kernel was calculated will result in an incorrect estimate of the cloud masking, and, by extension, the cloud feedbacks in the model in which the kernel is applied. Regions near the sea ice edge are particularly susceptible to this problem, as open ocean regions tend to be cloudier than sea-ice regions. The local masking effect of clouds would then depend on whether the grid point was sea-ice covered in the mean state of the GFDL model. Thus small differences in the edge of the sea-ice between the model in which the radiative kernel is calculated and the model in which the kernel is applied could plausibly create spurious cloud feedbacks along the sea-ice edge as we have found. Furthermore, the wide model diversity in high latitude cloud properties (e.g., Gorodetskaya et al. (2008)) exacerbates this problem.

In light of these considerations, we argue that the cloud radiative kernels developed here are more accurate in regions where surface albedo changes significantly, and we exclude from Figure 3 locations in which the magnitude of the change in clear-sky surface albedo exceeds the 90th percentile of all clear-sky surface albedo changes.

A potential limitation of the cloud radiative kernel technique developed here is the fact that it relies on simulated cloud fields that are only present for sunlit months in which a satellite sensor could retrieve visible optical depths. Only the sunlit portion of the diurnal cycle of cloudiness is sampled by the ISCCP simulator, and in polar regions, entire months are devoid of cloud information when the sun does not rise above the horizon. This is potentially problematic for diagnosing LW cloud feedback because cloud fields impact LW radiation at all times, not just when the sun is up. Thus, if the change in cloud properties between the $2xCO_2$ climate and the $1xCO_2$ climate is systematically different between night and day or between dark and sunlit seasons, this technique will be biased, capturing only the cloud changes that occur for sunlit months. We find that in the annual mean, the adjusted change in LW cloud forcing at high latitudes agrees to within 0.1 W m^{-2} K^{-1} of the value computed when only sunlit months are sampled, suggesting that this is not a major issue. Obviously the effect of simulator application to sunlit months has no effect on SW cloud feedback estimates, as cloud changes occurring when the sun is down do not impact SW radiative fluxes anyway.

In Figure 4 we show the cloud radiative kernel-derived computation of global mean LW, SW, and net cloud feedbacks scattered against the estimates derived using the adjusted change in cloud radiative forcing method. In the global mean, cloud kernel-derived estimates of LW cloud feedback tend to be larger than the adjusted change in LW cloud radiative

forcing ($\Delta LWCF$) cloud feedback (in five out of six models) whereas the SW cloud feedback estimates computed here fall evenly on either side of the one-to-one line when plotted against the adjusted $\Delta SWCF$ values. The net cloud feedbacks computed with the cloud radiative kernels generated here tend to overestimate the adjusted $\Delta NetCF$ cloud feedback, and this is primarily caused by discrepancies in the LW term. Cloud feedback estimates for the *uiuc* model stand out as particularly anomalous. It is noteworthy, however, that this model only appears anomalous when its cloud kernel-computed feedbacks are compared with the adjusted change in cloud radiative forcing, not when they are compared with the cloud kernel-computed feedbacks of the other models. That cloud feedbacks computed using the cloud radiative kernels (which rely on a standard radiative transfer code and a standard definition of cloud) are in better agreement across models than feedbacks computed from adjusting the change in cloud forcing (which relies in part on the cloud radiative forcing computed in each model's radiative transfer scheme) suggests that the discrepancy arises due to anomalous features of the *uiuc* model's radiative transfer scheme relative to the those of the other models and to that of the kernel. Indeed, Tsushima et al. (2006) noted that this model has the lowest cloud albedo forcing despite having the largest total water content among the 5 models they analyzed. In light of the anomalous behavior of the *uiuc* model apparent in Figure 3d and j and Figure 4, we exclude this model from any ensemble means, including those shown in Figure 2.

In Figure 5 we show the full spatial structure of the cloud feedbacks computed with the cloud radiative kernels (left column) and computed by adjusting the change in cloud forcing (middle column) averaged across the *ukmo_hadsm4*, *ukmo_hadsm3*, *ukmo_hadgsm1*, *miroc_losens*, and *cccma_agcm4_0* models. The difference maps are also provided in the

right column. The net cloud feedback is generally positive between 50°S and 65°N, exceptions being just south of the equator in the Eastern Pacific, in the subtropical Atlantic, and over the Tibetan Plateau. The low latitude signal is dominated by the SW cloud feedback, but the positive LW cloud feedback on the equator in the Pacific contributes significantly to the positive net cloud feedback there. Large positive SW cloud feedback outweighs large negative LW cloud feedback over the Amazon, in the South Pacific Convergence Zone and over southern Africa. Negative SW cloud feedback outweights positive LW cloud feedback in the regions south of 50°S and north of 65°N.

In general, the differences between cloud feedback estimates computed using the cloud radiative kernel developed here and the adjusted change in cloud radiative forcing are characterized by an overestimation of the magnitude of the local feedback value (i.e., the kernel value is greater where the feedback is positive and smaller where the feedback is negative). While the errors in the SW cloud feedback average out to nearly zero globally (both methods yield a global mean SW cloud feedback of 0.44 W m^{-2} K^{-1}), the LW cloud feedback is slightly overestimated using the cloud radiative kernel technique. Thus, the net cloud feedback calculated with the cloud radiative kernels is slightly larger (roughly 6% larger) that that calculated by the adjusted change in cloud forcing method. Still, we argue that this technique works remarkably well considering the myriad assumptions that are made in constructing cloud radiative kernel histograms. The great advantage of using cloud radiative kernels over other methods of computing cloud feedback is that it allows one to directly calculate the contributions of different cloud types to cloud feedback, as demonstrated in the following section.

6. Partitioning the Cloud Feedback by Cloud Types

The computed histograms allow one to directly attribute the contributions of specific cloud types to the cloud feedback at each location. In Figure 6 we show the zonal mean contribution of high, middle, and low clouds to the LW, SW, and net cloud feedbacks averaged across all twelve models except the *uiuc* and *mpi_echam5* models. As expected based on the fact that LW cloud forcing is greatest for high clouds, the LW cloud feedback is dominated at all latitudes by the response of high clouds (Figure 6a). Low cloud changes are irrelevant at all latitudes, but middle level cloud changes act to slightly reduce the LW cloud feedback in the midlatitudes. The results shown here add legitimacy to the assumptions made in Zelinka and Hartmann (2010) that low cloud changes have a negligible impact on OLR compared to high cloud changes.

In contrast, cloud fraction changes at all altitudes are relevant for SW cloud feedback at all latitudes (Figure 6b). With the exception of the high latitudes, changes in low and middle level clouds tend to contribute to a positive SW cloud feedback. High cloud changes contribute negatively to the SW cloud feedback in the global mean, but most prominently in the deep Tropics (due mainly to large increases over the Equatorial Pacific) and poleward of about 40° in both hemispheres. The effect of increases in high cloud fraction in the deep Tropics strongly opposes the effect of decreases in the other cloud types, producing a minimum value in the SW cloud feedback. Positive SW cloud feedbacks from middle level clouds are nearly 70% as large as those from low level clouds in the global mean, and are larger in the middle and high latitudes, a result that is not generally acknowledged and is frequently overshadowed by the focus on feedback spread arising from subtropical low cloud

changes[2].

The signs of each cloud type's contributions to the SW cloud feedback (i.e., negative for high clouds and positive for low and middle level clouds) are consistent with those found for the doubled CO_2 slab ocean experiments analyzed by Yokohata et al. (2010), who used the approximate partial radiative perturbation method of Taylor et al. (2007) in combination with ISCCP simulator output in two perturbed physics ensembles of the MIROC3.2 and HadSM3 models to separate the contribution of clouds at different altitudes to the SW cloud feedback.

Cloud changes in every height category contribute positively to the net cloud feedback (Figure 6c). Because of their largely compensatory effects on the SW and LW cloud feedbacks, high cloud changes contribute less than low cloud changes to the net cloud feedback at all latitudes. Mid-level cloud changes, which only appreciably contribute to the SW cloud feedback, contribute nearly the same amount to the global cloud feedback as high cloud changes and have a very similar latitudinal distribution, except in high southern latitudes. Middle- and high-level cloud changes together are responsible for more than half of the global and ensemble mean net cloud feedback.

[2]A well-known tendency of the ISCCP retrieval algorithm that is purposely built into the simulator is to identify a single cloud with a CTP at mid-levels for scenes in which thin high clouds overlap low clouds (e.g., Jin and Rossow (1997); Stubenrauch et al. (1999)). Motivated by a concern that the significant mid-level cloud feedback we have inferred may arise partly due to clouds that are not actually at mid-levels, we calculated high, middle, and low cloud amounts by averaging the cloud amount diagnostic provided by seven modelling centers within the 50-440 hPa, 440-680 hPa, and 680-1000 hPa pressure levels, respectively. Comparing maps of the sign of these cloud amount changes with the sign of the corresponding cloud fraction anomlies derived from the histograms (not shown), we found that 14% of all points exhibit mid-level cloud changes of opposite sign, which is comparable to the 13% for high clouds and 17% for low clouds. Furthermore, the number of gridpoints in which the signs are opposite and the histogram-derived mid-level cloud fraction anomalies are positive is roughly equal to those in which the histogram-derived mid-level cloud fraction anomalies are negative, implying no systematic disagreement. Although this is a crude comparison, it shows that, over the vast majority of gridpoints, middle-level cloud changes are indeed causing mid-level cloud feedbacks.

In Figure 7 we show the zonal mean contribution of thin, medium, and thick clouds to the LW, SW, and net cloud feedbacks for all twelve models except the *uiuc* and *mpi_echam5* models. In the global mean sense, thick clouds dominate the LW cloud feedback, particularly at high latitudes (Figure 7a). Clouds in all three thickness categories contribute equally to the large positive LW cloud feedback in the deep Tropics (7.5°S - 15°N), and cloud fraction changes in the thin and medium thickness categories tend to oppose cloud fraction changes in the thick category poleward of about 50° in either hemisphere.

In the global mean, the SW cloud feedback is dominated by the contribution from medium thickness cloud changes, which is positive everywhere but over the poles (Figure 7b). With the exception of the very high latitudes, thin cloud changes contribute minimally to the SW cloud feedback. The sharp decrease in the SW cloud feedback with latitude in the midlatitudes is entirely caused by increases in thick clouds and is generally opposed by smaller cloud fraction decreases in the other τ categories. Particularly striking is the negative feedback in the SH storm track region which reaches a peak value of -1.5 W m^{-2} K^{-1}, with thick cloud changes alone contributing -2.1 W m^{-2} K^{-1}.

It may be somewhat surprising that medium thickness cloud changes dominate over thick cloud changes for the global mean SW cloud feedback considering that SW flux sensitivity increases with τ, leading one to expect SW cloud feedback to be dominated by changes in thick clouds. However, it is clear from the latitudinal structure of the contributions that thick cloud fraction changes are at least as important at most latitudes as medium thickness cloud changes; the difference therefore arising from the fact that medium thickness cloud changes contribute positively almost everywhere whereas the thick cloud contribution is strongly positive equatorward of about 50° and negative elsewhere. It is interesting that

medium-thickness cloud changes contribute positively to SW cloud feedback at nearly every latitude.

Cloud fraction changes in all optical depth categories contribute positively to the net cloud feedback, with the medium thickness cloud changes dominating in the global mean due to their uniformly positive contributions (Figure 7c). Equatorward of about 45°, thick and medium thickness cloud changes contribute about equally to the net cloud feedback, with thick clouds primarily causing the abrupt latitudinal transition from positive to negative cloud feedback in the midlatitudes.

In Figure 8 we show global mean cloud feedback estimates and their partitioning among high, middle, and low clouds for all models except *uiuc* and *mpi_echam5*. In this ensemble of ten models, 65% of the net cloud feedback comes from the SW cloud feedback and 35% from the LW. For both the global mean SW and LW cloud feedbacks, only one model has negative values (not the same model). Considerable spread is evident in both the LW and SW components of cloud feedback, though it is larger in the SW. Anticorrelation between LW and SW cloud feedback estimates across models results in the net cloud feedback having less inter-model spread than that of SW cloud feedback.

As mentioned previously, LW cloud feedback is dominated by the response of high clouds, with middle and low clouds making small negative contributions. Clouds at all vertical levels contribute to the SW cloud feedback, with high clouds contributing negatively and middle and low cloud contributing positively. Considerable inter-model spread is evident in the contributions of clouds at all heights to the SW cloud feedback. High, middle, and low cloud changes all contribute positively to the net cloud feedback. The contribution of cloud changes at all heights to the net cloud feedback exhibits appreciable spread, but the spread

is largest for low clouds, a result consistent with many previous studies (e.g., Bony and Dufresne (2005)). An important and generally unappreciated result shown in Figure 8 is that the high cloud contribution to the inter-model spread in net cloud feedback is smaller than the contribution from low clouds not because the response of high clouds is small and/or consistent across models. Rather, the inter-model spread in the response of high clouds contributes substantial spread to both LW and SW cloud feedbacks. Specifically, the contributions of high cloud changes to LW and SW cloud feedbacks each span a range of about 1 W m^{-2} K^{-1}, whereas the contribution of low cloud changes to SW cloud feedback spans a range of only 0.67 W m^{-2} K^{-1}. Because the spread in high cloud-induced LW and SW components is partially compensatory, however, the spread in net cloud feedback induced by high cloud changes is smaller than that induced by low cloud changes, for which no such compensation occurs. The high cloud-induced SW cloud feedback represents the feedback component with the largest inter-model spread.

In Figure 9 we show global mean cloud feedback estimates and their partitioning among thin, medium, and thick clouds for all models except *uiuc* and *mpi_echam5*. Thin cloud changes generally make a small contribution to the feedback in all models. Thick clouds make a larger contribution to the positive LW cloud feedback than do medium thickness clouds, but the multi-model mean SW cloud feedback is dominated by medium thickness cloud reductions, with no contribution from thick cloud changes. Again, note that thick clouds make no contribution to the global mean SW cloud feedback because their lower latitude contribution exactly compensates their higher latitude contribution (Figure 7b). Interestingly, all models exhibit a positive contribution to SW cloud feedback from medium-thickness cloud changes, whereas roughly an equal number of models exhibit positive and

negative SW cloud feedback contributions from thick cloud changes. Conversely, all models exhibit positive contribution to LW cloud feedback from thick cloud changes, whereas roughly an equal number of models exhibit positive and negative LW cloud feedback contributions from medium-thickness cloud changes. The spread in SW cloud feedback due to both medium and thick cloud types is large, but because the SW cloud feedback is systematically positive for medium thickness clouds, it represents the largest positive contribution to the ensemble mean cloud feedback of all thickness categories. Indeed, the robust decrease in medium-thickness clouds is the single most important contributor to the ensemble mean positive net cloud feedback, larger than both the contribution of high cloud changes to the LW cloud feedback and the contribution of low cloud changes to the SW cloud feedback.

7. Conclusions

In this paper we demonstrated a new method of computing cloud feedbacks in models that output simulated cloud fractions as functions of cloud top pressure and cloud optical depth. ISCCP-simulated cloud fields have a distinct advantage over the standard cloud fraction profiles output by GCMs in that they are defined consistently across models and represent the "radiatively-relevant" cloud tops that are directly impacting TOA fluxes. The latter property allows us to compute TOA flux sensitivities for fluctuations in each cloud type. To do so, we insert cloud liquid and ice profiles appropriate for each individual CTP and τ bin in the ISCCP histogram into the Fu-Liou radiative transfer model. We consider this work an extension of the radiative kernel technique into cloud fields. Like the standard kernels of Soden et al. (2008), the cloud radiative kernels computed here are functions of

space and time (latitude, month, and pressure), but they have an additional dependence on cloud optical depth. Unlike the standard kernels, we did not compute kernels for every longitude, but rather for ten bins of surface albedo.

Cloud feedback is computed using the kernels in a similar manner to the computation of standard feedbacks as in Soden et al. (2008). Specifically, at every location in the model, the change in cloud fraction in each CTP-τ bin between the doubled CO_2 run and control run is multiplied by the corresponding bin of the cloud radiative kernel. The feedback is computed by summing over all bins of the histogram and dividing by the global mean temperature change.

Several appealing aspects of this technique are worth highlighting. First, cloud feedbacks are computed directly from the change in cloud fields, which means the contributions to the feedback from specific cloud types are computed rather than inferred. Second, cloud feedbacks are computed using the same kernel across models, which isolates the role of cloud changes in driving intermodel differences in feedback values, without any model-to-model variation in the radiative code computing the feedback. Third, monthly mean ISCCP simulator output is all that is needed to compute the feedback, which makes it a very straightforward calculation, one that does not require extracting instantaneous cloud output in order to implement the partial radiative perturbation technique or adjusting the change in cloud forcing by the amount of masking in all other feedbacks. Finally, clear-sky changes that are irrelevant for cloud feedback but may be difficult to remove using other techniques are easily avoided in the computation, resulting in TOA flux anomalies that are solely due to changes in the cloud fraction histogram.

We have demonstrated that cloud feedbacks computed with the cloud radiative kernels

compare favorably with values computed by adjusting the change in cloud radiative forcing (Soden et al. (2008)). This is especially true for SW cloud feedbacks, as the LW and net cloud feedbacks are generally slightly overestimated relative to the adjusted change in cloud forcing. On a point-by-point basis, cloud feedbacks computed using the two methods agree closely, nearly following a one-to-one line (except in the SW for the *uiuc* model) with high correlation in every model except the *miroc_losens* model.

We find that changes in high clouds make the largest contribution of any cloud type to the LW cloud feedback at all latitudes in the ten model ensemble mean, especially in the deep tropics. This is consistent with the structure of the LW cloud kernel, which indicates that the sensitivity of OLR to cloud fraction changes increases with decreasing cloud top pressure. However, because high cloud increases contribute negatively to the SW cloud feedback, their contribution to the net cloud feedback is considerably reduced. In contrast, low cloud changes, which only impact the SW cloud feedback, make up a larger contribution to the net cloud feedback than cloud fraction changes at other altitudes. However, it is important to bear in mind that even for the net cloud feedback, the positive contribution from the sum of middle- and high-level topped clouds slightly exceed the contribution from low level clouds in the global mean. Furthermore, that the spread in net cloud feedback is dominated by the contribution from low clouds should not be taken as evidence that high cloud changes have either a small or consistent impact on radiative fluxes across models. Rather, high cloud changes induce an even wider range of contributions to SW and LW cloud feedbacks than do low cloud changes, but partial compensation between the LW and SW impacts of high cloud changes reduces their contribution to the spread in net cloud feedback relative to low cloud changes, whose impacts in the SW are not offset in the LW.

Cloud changes in all thicknesses categories contribute positively to the net cloud feedback, and increases in thick clouds at high latitudes in either hemisphere cause the rapid decrease of SW and net cloud feedbacks with latitude poleward of about 50°. Although they exhibit considerable inter-model spread, contributions to SW and net cloud feedback from medium thickness clouds are systematically positive across models, which results in medium-thickness cloud changes representing the single most important contributor to the net cloud feedback.

In the companion to this paper, we propose a technique to decompose the change in cloud fraction within the ISCCP simulator histograms in such a way as to isolate the contributions to cloud feedback from changes in cloud amount, height, and optical thickness. This decomposition is performed to highlight the nature of cloud changes that give rise to cloud feedbacks, and provides an indication of the physical processes that are important for both the mean and spread in cloud feedback across models.

Acknowledgments.

This research was supported by the Regional and Global Climate Program of the Office of Science at the U. S. Department of Energy and by NASA Grant NNX09AH73G at the University of Washington. We acknowledge the international modeling groups, the Program for Climate Model Diagnosis and Intercomparison (PCMDI), and the WCRP's Working Group on Coupled Modelling (WGCM) for their roles in making available the WCRP CFMIP multi-model dataset. Support of this dataset is provided by the Office of Science, U.S. Department of Energy. We thank Brian Soden for providing the radiative kernels, Rick Hemler for providing additional *gfdl_mlm2_1* model output, Rob Wood, Chris

Bretherton, and Robert Pincus for useful discussion and suggestions for improvement, and Marc Michelsen for computer support. This work was performed under the auspices of the U.S. Department of Energy by Lawrence Livermore National Laboratory under Contract DE-AC52-07NA27344.

APPENDIX

Verification of Proper ISCCP Simulator Implementation

a. Consistency Between Measures of Total Cloud Fraction

Among the checks that modeling centers are expected to perform to ensure proper implementation of the ISCCP simulator is to verify that the total cloud fraction computed by summing the CTP-τ histogram is the same as the total cloud fraction diagnostic computed by the GCM cloud scheme. We have performed this check and found RMS differences between the two fields are 8% in the *ipsl_cm4* model, 4% in the *ncar_ccsm3_0* model, and less than 2% in the *ukmo_hadsm4*, *ukmo_hadsm3*, *ukmo_hadgsm1*, *uiuc*, and *cccma_agcm4_0* models.

In two models (*bmrc1* and *miroc_hisens*), the total cloud fraction diagnostic is not reported, so no comparison could be made. Since the cloud feedbacks computed for these two models also cannot be "ground-truthed" against the adjusted change in cloud forcing method, we cannot verify that the simulator is implemented properly in these models. However, in an effort to keep a reasonably-sized ensemble of models in our analysis, we take on faith that they have properly implemented the simulator. It is somewhat reassuring that their cloud fraction histograms are not anomalous relative to the ensemble mean (once the correction

described below is made for the *miroc_hisens* model).

We found that the CTP-τ histogram for the *gfdl_mlm2_1* model archived in the CFMIP1 database had not been divided by the fraction of radiation time steps with sunlit conditions, resulting in a large underestimate of total cloud fraction as well as features resulting from sampling only the sunlight points in a given month. Dividing by the fraction of calls to the simulator in each month with sunlit conditions (data field provided by R. Hemler) brought the total cloud fractions into agreement, with an RMS difference of roughly 1%.

Total cloud fraction computed by summing the CTP-τ histogram of the *miroc_losens* model greatly overestimated the total cloud fraction diagnostic. Both *miroc* models have an anomalously large cloud fraction in the highest, thinnest bin relative to the other models, possibly indicating that "trivial" clouds (e.g. clouds having cloud water contents less than 10^{-8} kg kg^{-1} but greater than zero which might result from numerical errors in the advection of positive definite and highly inhomogeneous fields) are getting counted as cloud by the simulator whereas the total cloud diagnostic in this model would not record a cloud as being present. Artificially setting cloud fraction in the highest, thinnest bin to zero brought the two estimates of total cloud fraction into agreement, with an RMS difference of roughly 4.5% in the *miroc_losens* model that is dominated by differences over Antarctica. Removal of clouds in the highest, thinnest bin has a negligible effect on the resultant feedback computed for both *miroc* models because of the relative insensitivity of radiative fluxes to this very thin cloud type.

The 4% RMS difference in the two computations of total cloud fraction in the *ncar_ccsm3_0* model does not reflect incorrect simulator implementation, but rather the presence of "empty clouds" that are recorded by the model's cloud amount diagnostic but not by the simulator.

Such "clouds" contain no or very little liquid water and are present due to the diagnostic cloud fraction being computed separately from the prognostic cloud water in CAM (Hannay et al.). In these situations, the simulator is providing the true radiatively-relevant clouds.

Finally, we have chosen to exclude the *mpi_echam5* model from our analysis based on two considerations. First, the total cloud fraction computed by summing its CTP-τ histogram is significantly different from the total cloud fraction diagnostic, with an RMS difference of 30.5%. The total cloud fraction as computed by summing the histogram is rarely less than 80% at any location on the planet, resulting in a global mean total cloud fraction of 92% that is highly inconsistent with the total cloud fraction diagnostic. Second, the RMS difference between this model's CTP-τ histogram and the ensemble mean histogram is larger than for any other model in the ensemble, with values exceeding 10% in several bins. Williams and Webb (2009) have also noted that among the ten models they analyzed, the *mpi_echam5* model's histogram has the largest Euclidean distance to ISCCP observations in several cloud regimes.

b. Consistency Between Clouds and Radiation

Unlike the typical implementation of the ISCCP simulator in which the cloud fields reported in the histogram represent those for which the radiative transfer calculations are performed, in the *cccma_agcm4_0* model, the cloud fields reported in the ISCCP simulator histogram are different from those used by the model's radiation code (J. Cole, personal communication, 2011). In this model's radiation calculations, cloud visible optical depths are scaled down according to Eq. 12 of Li et al. (2005) to account for subgrid-scale inhomogeneity

in the cloud fields that strongly impacts scattering (Li (2000); Li and Barker (2002)). Because the ISCCP simulator is called prior to this scaling, the cloud fields reported in the histogram do not represent the same clouds as seen by that model's radiation code. Thus, the GCM-produced radiative fluxes are guaranteed to be inconsistent with those computed using the cloud radiative kernels applied to ISCCP simulator output because the kernels assume the clouds in the histogram are those seen by the radiation. To circumvent this problem, for this model only we log-linearly interpolate the values of the cloud radiative kernels from the original optical depths of the ISCCP simulator to optical depths that have been scaled according to Eq. 12 of Li et al. (2005). Applying this scaling reduced the slope shown in Figure 3l from 1.50 to 1.06, significantly improving the agreement between the SW cloud feedback calculated with the cloud kernel and that calculated by adjusting the change in $SWCF$.

This scaling was not applied for LW radiation in the *cccma_agcm4_0* model. Although the code does take into account the effect of horizontal variability in cloud fields on LW radiative transfer, it is not a simple modification of the optical thickness since the inhomogeneity was developed right into the radiative transfer solution (J. Cole, personal communication, 2011). Nevertheless, we scale the LW cloud radiative kernel in the same manner as the SW radiative kernel. This slightly improved the agreement between the cloud radiative kernel- and adjusted change in LW cloud forcing-computed feedbacks, with the slope shown in Figure 3f decreasing from 1.35 to 1.22.

REFERENCES

Ackerman, T. P., K. N. Liou, F. P. J. Valero, and L. Pfister, 1988: Heating rates in tropical anvils. *J. Atmos. Sci.*, **45**, 1606–1623.

Bony, S. and J. L. Dufresne, 2005: Marine boundary layer clouds at the heart of tropical cloud feedback uncertainties in climate models. *Geophys. Res. Lett.*, **32**, L20806, doi: 10.1029/2005GL023851.

Bony, S., J. L. Dufresne, H. L. Treut, J. J. Morcrette, and C. Senior, 2004: On dynamic and thermodynamic components of cloud changes. *Climate Dyn.*, **22**, 71–68.

Cess, R. D. e. a., 1990: Intercomparison and interpretation of cloud-climate feedback processes in nineteen atmospheric general circulation models. *J. Geophys. Res.*, **95**, 16 601–16 615.

Charlock, T. P. and V. Ramanathan, 1985: The albedo field and cloud radiative forcing produced by a general circulation model with internally generated cloud optics. *J. Atmos. Sci.*, **42**, 1408–1429.

Colman, R. and B. McAvaney, 2011: On tropospheric adjustment to forcing and climate feedbacks. *Climate Dyn.*, 1–10.

Fu, Q., 1996: An accurate parameterization of the solar radiative properties of cirrus clouds for climate models. *J. Climate*, **9**, 2058–2082.

Fu, Q. and K. N. Liou, 1992: On the correlated k-distribution method for radiative transfer in nonhomogeneous atmospheres. *J. Atmos. Sci.*, **49**, 2139–2156.

Gorodetskaya, I. V., L. B. Tremblay, B. Liepert, M. A. Cane, and R. I. Cullather, 2008: The influence of cloud and surface properties on the Arctic Ocean shortwave radiation budget in coupled models. *J. Climate*, **21 (5)**, 866–882.

Gregory, J. and M. Webb, 2008: Tropospheric adjustment induces a cloud component in CO2 forcing. *J. Climate*, **21 (1)**, 58–71.

Hannay, C., D. L. Williamson, J. J. Hack, J. T. Kiehl, J. G. Olson, S. A. Klein, C. S. Bretherton, and M. Khler, ????: Evaluation of forecasted southeast pacific stratocumulus in the NCAR, GFDL, and ECMWF models. *J. Climate*, **22 (11)**, 2871–2889.

Harrison, E. F., P. Minnis, B. R. Barkstrom, V. Ramanathan, R. D. Cess, and G. G. Gibson, 1990: Seasonal variation of cloud radiative forcing derived from the Earth Radiation Budget Experiment. *J. Geophys. Res.*, **95**, 18 678–18 703.

Hartmann, D. L., L. A. Moy, and Q. Fu, 2001: Tropical convection and the energy balance at the top of the atmosphere. *J. Climate*, **14**, 4495–4511.

Jin, Y. and W. B. Rossow, 1997: Detection of cirrus overlapping low-level clouds. *J. Geophys. Res.*, **102**, 1727–1737, doi:10.1029/96JD02996.

Klein, S. A. and C. Jakob, 1999: Validation and sensitivities of frontal clouds simulated by the ECMWF model. *Mon. Weath. Rev.*, **127**, 2514–2531.

Kubar, T. L., D. L. Hartmann, and R. Wood, 2007: Radiative and convective driving of tropical high clouds. *J. Climate*, **20**, 5510–5526.

Li, J., 2000: Accounting for overlap of fractional cloud in infrared radiation. *Quart. J. Roy. Meteor. Soc.*, **126**.

Li, J. and H. W. Barker, 2002: Accounting for unresolved clouds in a 1D infrared radiative transfer model. Part II: Horizontal variability of cloud water path. *J. Atmos. Sci.*, **59 (23)**, 3321–3339.

Li, J., S. Dobbie, P. Risnen, and Q. Min, 2005: Accounting for unresolved clouds in a 1-D solar radiative-transfer model. *Quart. J. Roy. Meteor. Soc.*, **131 (608)**, 1607–1629.

McAvaney, B. J. and H. Le Treut, 2003: The cloud feedback intercomparison project: (CFMIP). *CLIVAR Exchanges 26, supplementary contributions.*

Ringer, M. A., et al., 2006: Global mean cloud feedbacks in idealized climate change experiments. *Geophys. Res. Lett.*, **33**, L07718, doi:10.1029/2005GL025370.

Rossow, W. B. and R. A. Schiffer, 1999: Advances in understanding clouds from ISCCP. *Bull. Amer. Meteor. Soc.*, **80 (11)**, 2261–2287.

Slingo, A., 1989: A GCM parameterization for the shortwave radiative properties of water clouds. *J. Atmos. Sci.*, **46 (10)**, 1419–1427.

Soden, B. J., A. J. Broccoli, and R. S. Hemler, 2004: On the use of cloud forcing to estimate cloud feedback. *J. Climate*, **17**, 3661–3665.

Soden, B. J. and I. M. Held, 2006: An assessment of climate feedbacks in coupled ocean-atmosphere models. *J. Climate*, **19**, 3354–3360.

Soden, B. J., I. M. Held, R. Colman, K. M. Shell, J. T. Kiehl, and C. A. Shields, 2008: Quantifying climate feedbacks using radiative kernels. *J. Climate*, **21**, 3504–3520.

Stubenrauch, C. J., W. B. Rossow, F. C. abd A. Chdin, and N. A. Scott, 1999: Clouds as seen by satellite sounders (3I) and imagers (ISCCP). Part I: Evaluation of cloud parameters. *J. Climate*, **12**, 2189–2213.

Taylor, K. E., M. Crucifix, P. Braconnot, C. D. Hewitt, C. Doutriaux, A. J. Broccoli, J. F. B. Mitchell, and M. J. Webb, 2007: Estimating shortwave radiative forcing and response in climate models. *J. Climate*, **20 (11)**, 2530–2543.

Tsushima, Y., et al., 2006: Importance of the mixed-phase cloud distribution in the control climate for assessing the response of clouds to carbon dioxide increase: A multi-model study. *Climate Dyn.*, **27**, 113–126.

Webb, M., C. Senior, S. Bony, and J. J. Morcrette, 2001: Combining ERBE and ISCCP data to assess clouds in the Hadley Centre, ECMWF and LMD atmospheric climate models. *Climate Dyn.*, **17**, 905–922.

Webb, M. J., et al., 2006: On the contribution of local feedback mechanisms to the range of climate sensitivity in two gcm ensembles. *Climate Dyn.*, **27**, 17–38.

Wetherald, R. and S. Manabe, 1988: Cloud feedback processes in a general circulation model. *J. Atmos. Sci.*, **45**, 1397–1415.

Williams, K. and G. Tselioudis, 2007: GCM intercomparison of global cloud regimes: present-day evaluation and climate change response. *Climate Dyn.*, **29**, 231–250.

Williams, K. and M. Webb, 2009: A quantitative performance assessment of cloud regimes in climate models. *Climate Dyn.*, **33**, 141–157.

Wyant, M. C., C. S. Bretherton, J. T. Bacmeister, J. T. Kiehl, I. M. Held, M. Zhao, S. A. Klein, and B. J. Soden, 2006: A comparison of low-latitude cloud properties and responses in agcms sorted into regimes using mid-tropospheric vertical velocity. *Climate Dyn.*, **27**, 261–279.

Yokohata, T., M. J. Webb, M. Collins, K. D. Williams, M. Yoshimori, J. C. Hargreaves, and J. D. Annan, 2010: Structural similarities and differences in climate responses to CO2 increase between two perturbed physics ensembles. *J. Climate*, **23 (6)**, 1392–1410.

Zelinka, M. D. and D. L. Hartmann, 2010: Why is longwave cloud feedback positive? *J. Geophys. Res.*, **115**, D16117, doi:10.1029/2010JD013817.

List of Tables

1 Global climate models that took part in the Cloud Feedback Model Intercomparison Project. Asterisks denote models for which profiles of atmospheric temperature and specific humidity were not provided. 45

Table 1. Global climate models that took part in the Cloud Feedback Model Intercomparison Project. Asterisks denote models for which profiles of atmospheric temperature and specific humidity were not provided.

#	Abbreviation	Modeling Center	Country
1	ukmo_hadsm4	Hadley Centre for Climate Prediction and Research / Met Office	U.K.
2	ukmo_hadsm3	Hadley Centre for Climate Prediction and Research / Met Office	U.K.
3	ukmo_hadgsm1	Hadley Centre for Climate Prediction and Research / Met Office	U.K.
4	uiuc	University of Illinois at Urbana-Champaign	U.S.A.
5	miroc_losens	Center for Climate System Research (The University of Tokyo), National Institute for Environmental Studies, and Frontier Research Center for Global Change	Japan
6	cccma_agcm4_0	Canadian Centre for Climate Modelling and Analysis	Canada
7	bmrc1*	Bureau of Meteorology Research Centre	Australia
8	gfdl_mlm2_1*	US Dept. of Commerce / NOAA / Geophysical Fluid Dynamics Laboratory	U.S.A.
9	ipsl_cm4*	Institut Pierre Simon Laplace	France
10	miroc_hisens*	Center for Climate System Research (The University of Tokyo), National Institute for Environmental Studies, and Frontier Research Center for Global Change	Japan
11	mpi_echam5*	Max Planck Institute for Meteorology	Germany
12	ncar_ccsm3_0*	National Center for Atmospheric Research	U.S.A.

List of Figures

1 Global and annual mean (a) LW, (b) SW, and (c) net cloud radiative kernels. The kernels have been mapped to the control climate's clear-sky surface albedo distribution before averaging in space; thus the average kernels are weighted by the actual global distribution of clear-sky surface albedo. 49

2 Global mean cloud fraction for the (a) 1xCO_2 and (b) 2xCO_2 runs of the *ukmo_hadsm4*, *ukmo_hadsm3*, *ukmo_hadgsm1*, *miroc_losens*, and *cccma_agcm4_0* models, along with (c) the difference expressed per unit change in each model's global mean surface temperature between the two states. Histogram resulting from multiplying the change in cloud fraction histogram at each location with the (d) LW, (e) SW, and (f) net cloud radiative kernel histogram, then taking a global mean. The sum of each histogram is shown in each title. For the feedbacks, the estimate computed using the adjusted ΔCRF technique of Soden et al. (2008) is also shown in the title. 50

3 Point-by-point comparison of (a-f) LW and (g-l) SW cloud feedbacks estimated from adjusting the change in cloud radiative forcing as in Soden et al. (2008) (x-axis) plotted against those estimated using the cloud radiative kernels developed here (y-axis). Locations in which the magnitude of the change in clear-sky surface albedo exceeds the 90th percentile have been removed. The thin line is the one-to-one line and the thick line is the linear least-squares fit to the data. The slope and 2σ range of uncertainty of this regression line along with the fraction of variance explained by the fit are provided in each panel. The uncertainty is calculated from a bootstrapping method in which the predictand is re-sampled 1000 times to compute a distribution of possible regression coefficients. 51

4 Global mean (a) LW, (b) SW, and (c) net cloud feedbacks for the (1) *ukmo_hadsm4*, (2) *ukmo_hadsm3*, (3) *ukmo_hadgsm1*, (4) *uiuc*, (5) *miroc_losens*, and (6) *cccma_agcm4_0* models estimated using the cloud radiative kernels developed here (y-axis) plotted against the estimates from adjusting the change in cloud radiative forcing as in Soden et al. (2008) (x-axis). The dashed line is the one-to-one line. Note that the x-axis and y-axis limits vary from panel to panel, but all span a range of 1 W m^{-2} K^{-1}. 52

5 (left column) Cloud kernel-derived and (middle column) adjusted change in cloud forcing-derived estimates of (top) LW, (middle), SW, and (bottom) net cloud feedback, along with (right column) the difference between the two estimates. The ensemble mean cloud feedback maps are computed only for models in which the standard kernel calculation is possible but excluding the *uiuc* model (i.e., the *ukmo_hadsm4*, *ukmo_hadsm3*, *ukmo_hadgsm1*, *miroc_losens*, and *cccma_agcm4_0* models). 53

6 Zonal mean ensemble mean (a) LW, (b) SW, and (c) net cloud feedbacks partitioned into contributions from high, middle, and low clouds. Global mean values of each contribution are shown in the legend. The abscissa is sine of latitude so that the visual integral is proportional to Watts per Kelvin of mean surface temperature change. The ensemble mean refers to all models except the *uiuc* and *mpi_echam5* models. 54

7 As in Figure 6, but partitioned into contributions from thin, medium, and thick clouds. 55

8 Global mean (red) LW, (blue) SW, and (black) net cloud feedback estimates and the contribution to the cloud feedbacks from high, middle, and low clouds. Each model is represented by a dot and the multi-model mean is represented by the height of the vertical bar. The *uiuc* and *mpi_echam5* models are excluded from this figure. 56

9 As in Figure 8, but partitioned into contributions from thin, medium, and thick clouds. 57

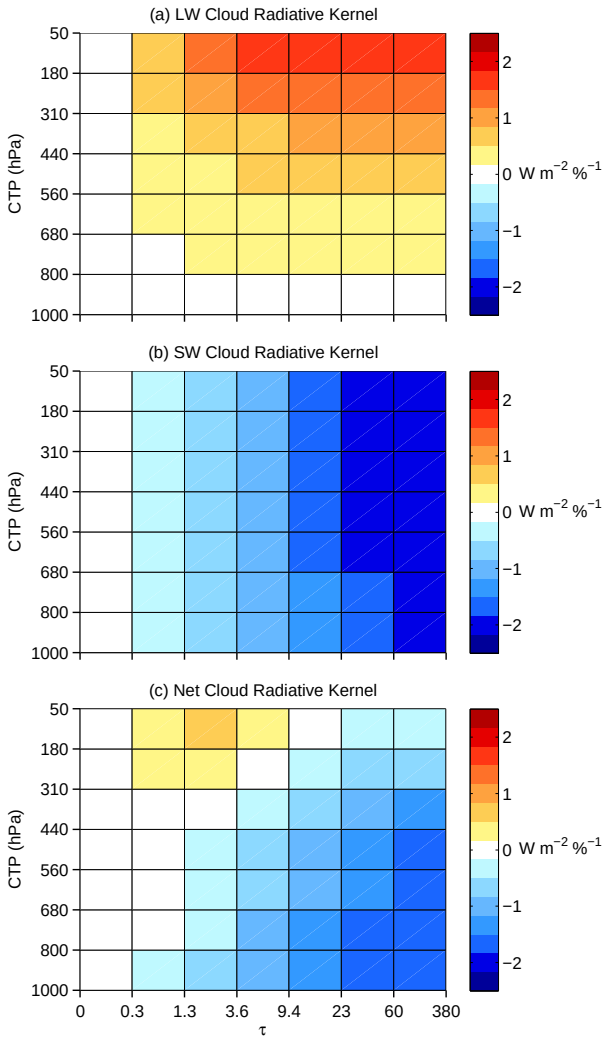

FIG. 1. Global and annual mean (a) LW, (b) SW, and (c) net cloud radiative kernels. The kernels have been mapped to the control climate's clear-sky surface albedo distribution before averaging in space; thus the average kernels are weighted by the actual global distribution of clear-sky surface albedo.

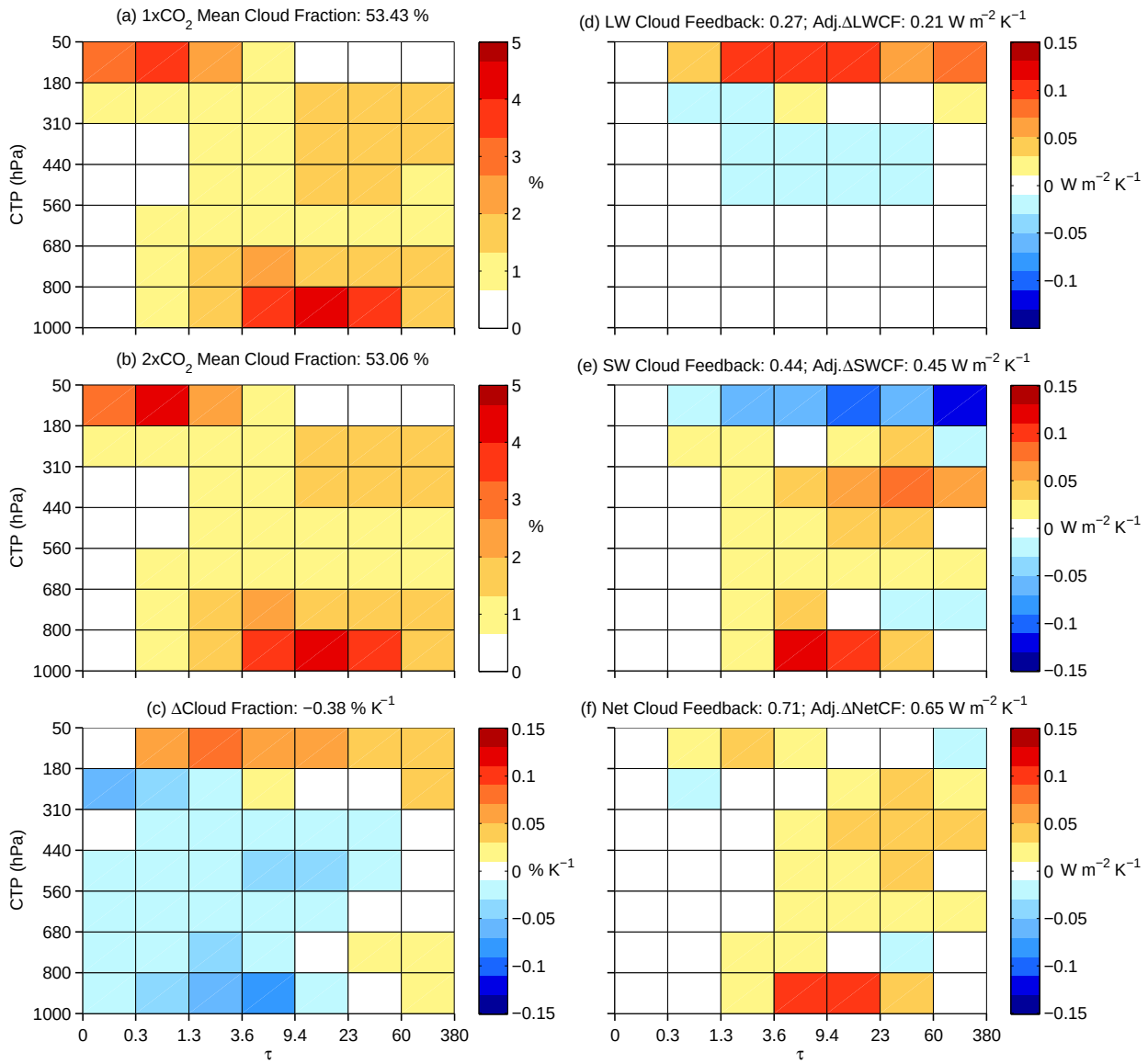

FIG. 2. Global mean cloud fraction for the (a) $1xCO_2$ and (b) $2xCO_2$ runs of the *ukmo_hadsm4*, *ukmo_hadsm3*, *ukmo_hadgsm1*, *miroc_losens*, and *cccma_agcm4_0* models, along with (c) the difference expressed per unit change in each model's global mean surface temperature between the two states. Histogram resulting from multiplying the change in cloud fraction histogram at each location with the (d) LW, (e) SW, and (f) net cloud radiative kernel histogram, then taking a global mean. The sum of each histogram is shown in each title. For the feedbacks, the estimate computed using the adjusted ΔCRF technique of Soden et al. (2008) is also shown in the title.

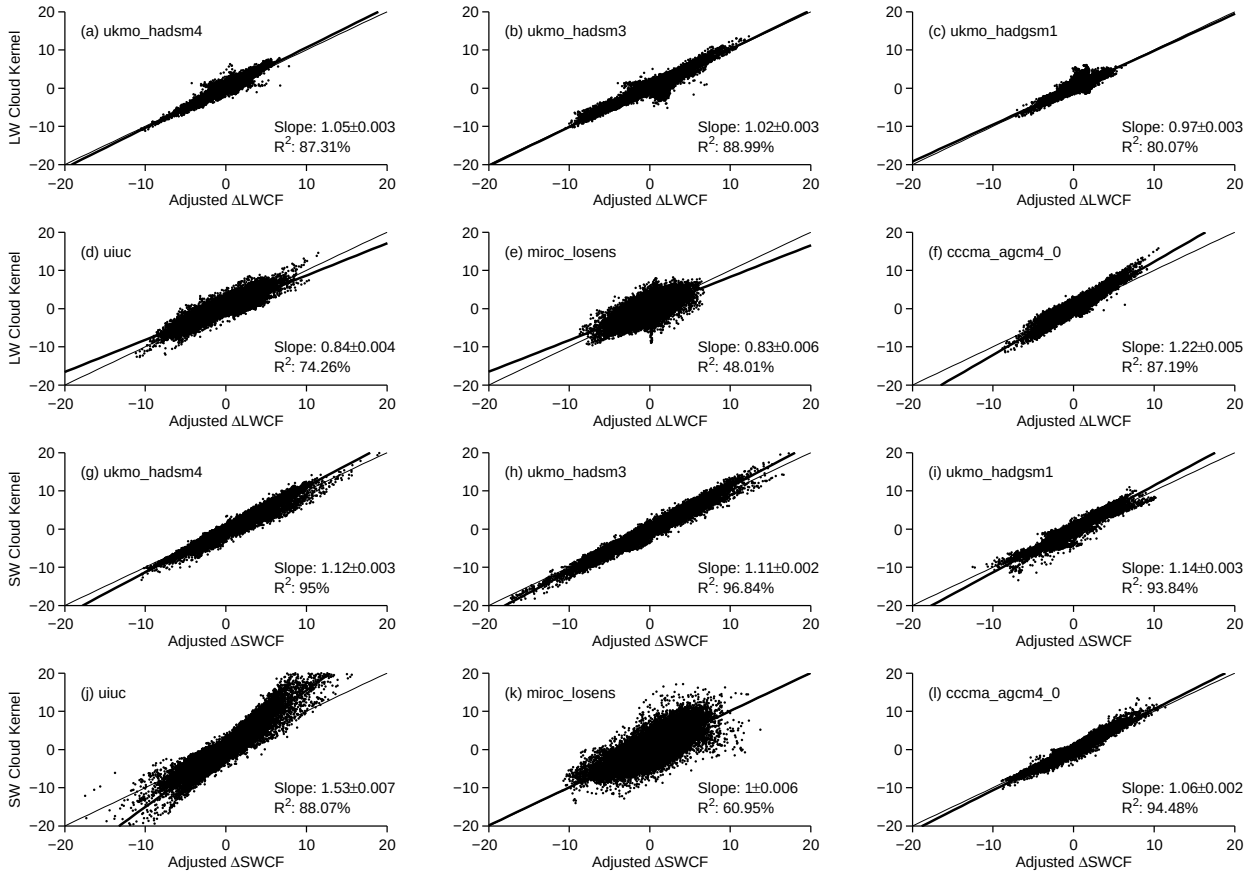

FIG. 3. Point-by-point comparison of (a-f) LW and (g-l) SW cloud feedbacks estimated from adjusting the change in cloud radiative forcing as in Soden et al. (2008) (x-axis) plotted against those estimated using the cloud radiative kernels developed here (y-axis). Locations in which the magnitude of the change in clear-sky surface albedo exceeds the 90th percentile have been removed. The thin line is the one-to-one line and the thick line is the linear least-squares fit to the data. The slope and 2σ range of uncertainty of this regression line along with the fraction of variance explained by the fit are provided in each panel. The uncertainty is calculated from a bootstrapping method in which the predictand is re-sampled 1000 times to compute a distribution of possible regression coefficients.

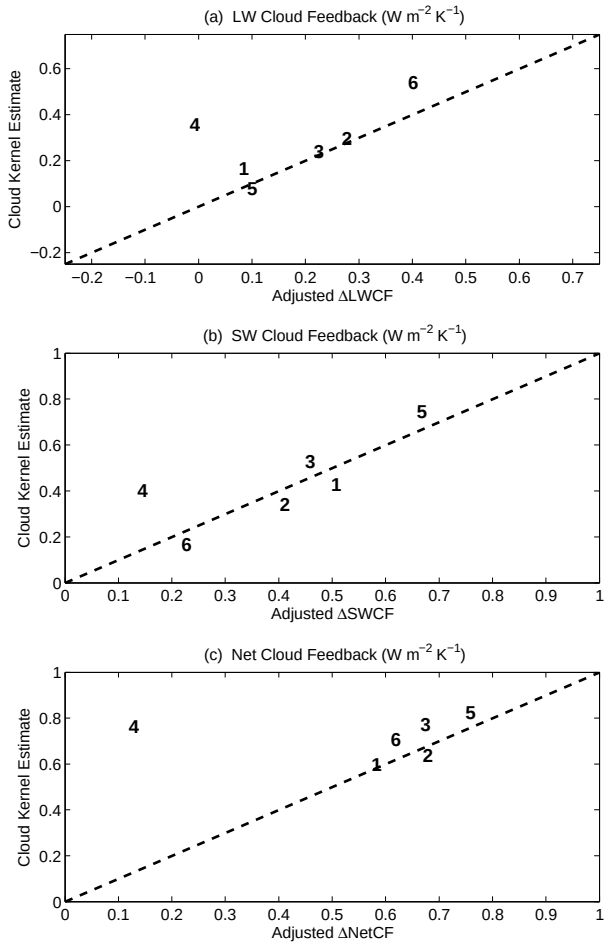

FIG. 4. Global mean (a) LW, (b) SW, and (c) net cloud feedbacks for the (1) *ukmo_hadsm4*, (2) *ukmo_hadsm3*, (3) *ukmo_hadgsm1*, (4) *uiuc*, (5) *miroc_losens*, and (6) *cccma_agcm4_0* models estimated using the cloud radiative kernels developed here (y-axis) plotted against the estimates from adjusting the change in cloud radiative forcing as in Soden et al. (2008) (x-axis). The dashed line is the one-to-one line. Note that the x-axis and y-axis limits vary from panel to panel, but all span a range of 1 W m^{-2} K^{-1}.

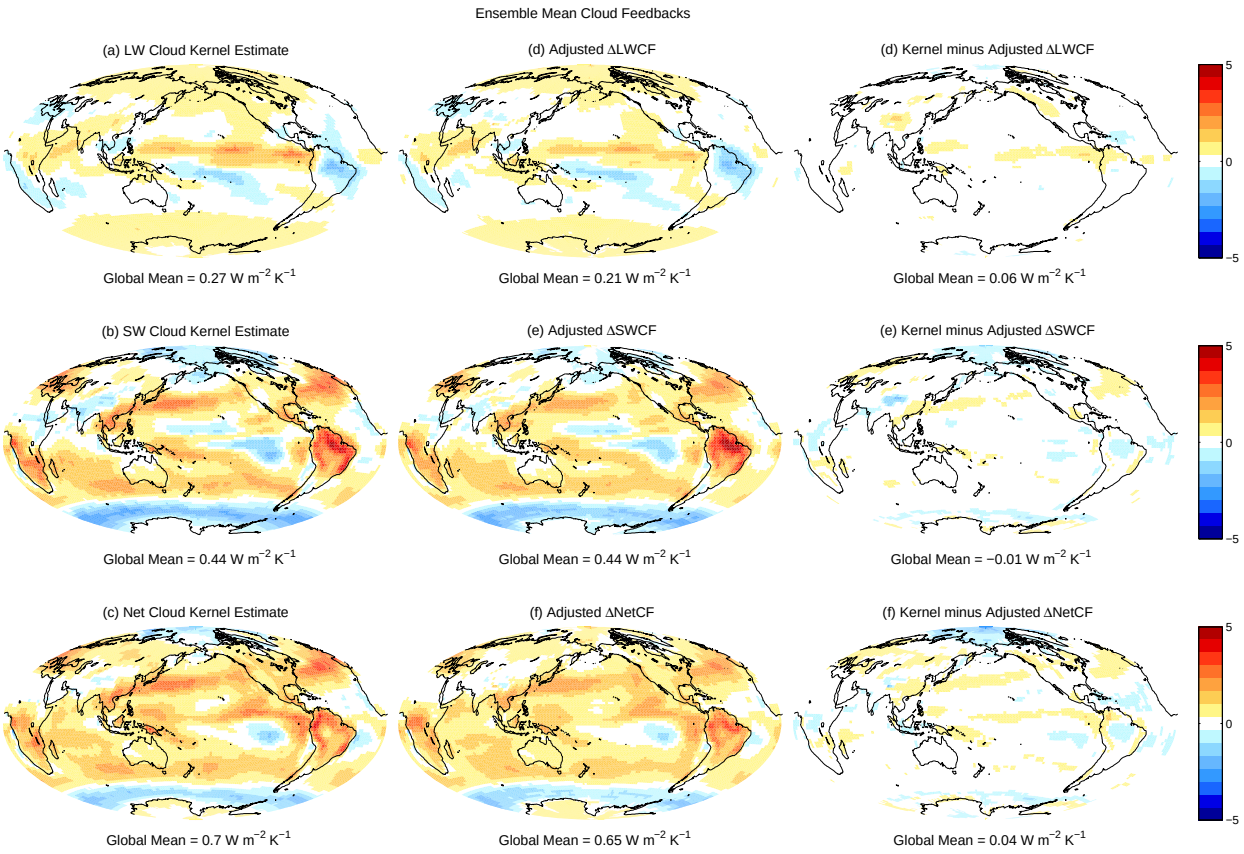

FIG. 5. (left column) Cloud kernel-derived and (middle column) adjusted change in cloud forcing-derived estimates of (top) LW, (middle), SW, and (bottom) net cloud feedback, along with (right column) the difference between the two estimates. The ensemble mean cloud feedback maps are computed only for models in which the standard kernel calculation is possible but excluding the *uiuc* model (i.e., the *ukmo_hadsm4*, *ukmo_hadsm3*, *ukmo_hadgsm1*, *miroc_losens*, and *cccma_agcm4_0* models).

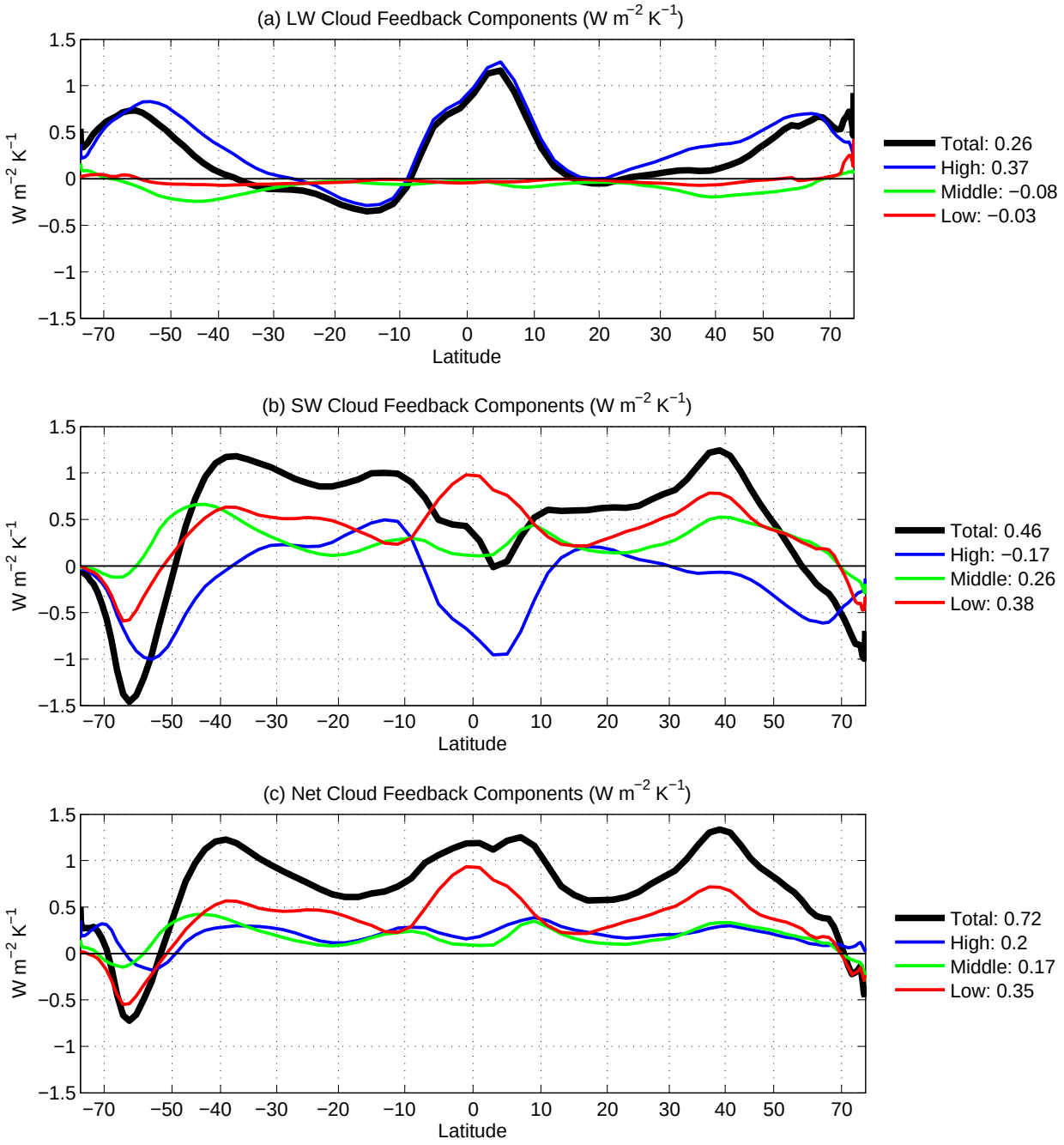

FIG. 6. Zonal mean ensemble mean (a) LW, (b) SW, and (c) net cloud feedbacks partitioned into contributions from high, middle, and low clouds. Global mean values of each contribution are shown in the legend. The abscissa is sine of latitude so that the visual integral is proportional to Watts per Kelvin of mean surface temperature change. The ensemble mean refers to all models except the *uiuc* and *mpi_echam5* models.

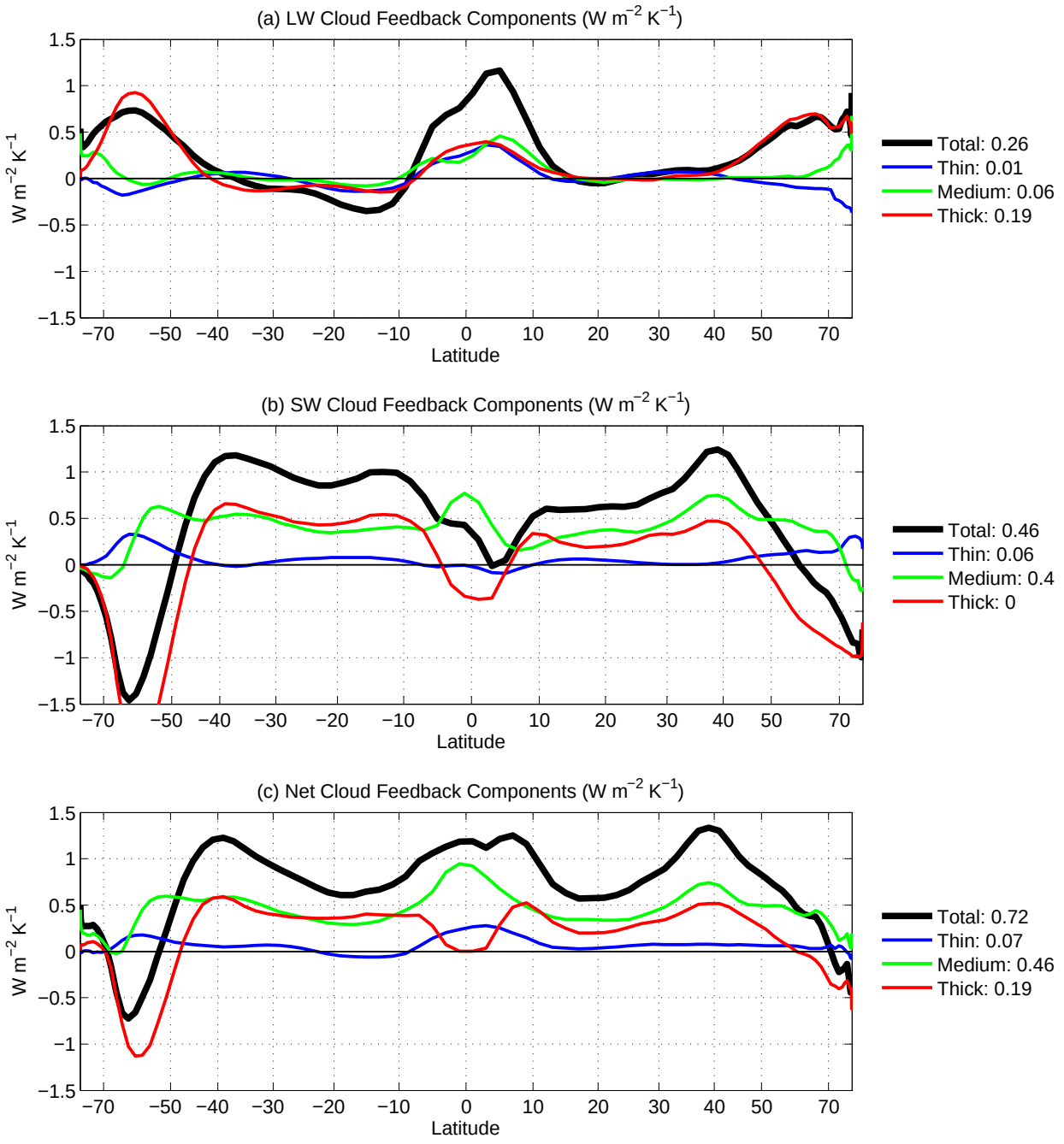

FIG. 7. As in Figure 6, but partitioned into contributions from thin, medium, and thick clouds.

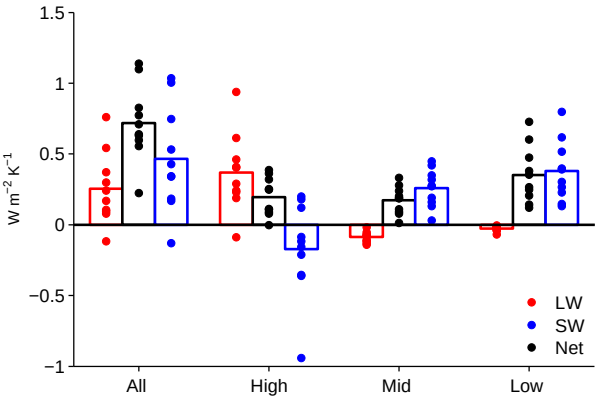

FIG. 8. Global mean (red) LW, (blue) SW, and (black) net cloud feedback estimates and the contribution to the cloud feedbacks from high, middle, and low clouds. Each model is represented by a dot and the multi-model mean is represented by the height of the vertical bar. The *uiuc* and *mpi_echam5* models are excluded from this figure.

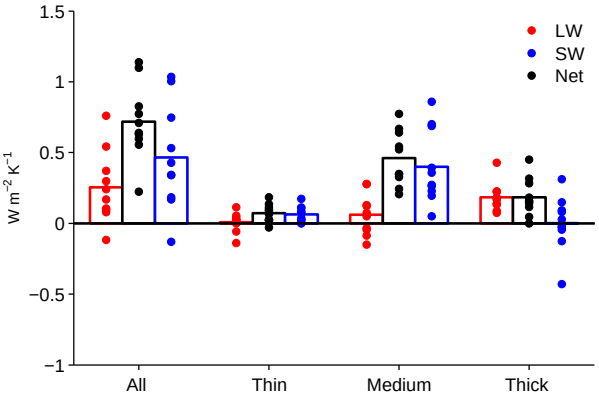

FIG. 9. As in Figure 8, but partitioned into contributions from thin, medium, and thick clouds.